Stratospheric photolysis frequencies: Impact of an improved numerical solution of the radiative transfer equation

Gaby Becker, Jens-Uwe Grooß, Daniel S. McKenna, and Rolf Müller[1]

Institute for Stratospheric Chemistry (ICG-1),
Forschungszentrum Jülich, 52425 Jülich, Germany,
(e-mail: ro.mueller@fz-juelich.de)

Citation: Becker, Gaby; Grooß, Jens-Uwe; McKenna, Daniel S.; Müller, Rolf, Stratospheric Photolysis Frequencies: Impact of an Improved Numerical Solution of the Radiative Transfer Equation, Journal of Atmospheric Chemistry, 37 (2000), 3, doi=10.1023/A:1006468926530

29 March 2000

Abstract

Numerical schemes for the calculation of photolysis rates are usually employed in simulations of stratospheric chemistry. Here, we present an improvement of the treatment of the diffuse actinic flux in a widely used stratospheric photolysis scheme (*Lary and Pyle, J. Atmos. Chem.*, 1991). We discuss both the consequences of this improvement and the correction of an error present in earlier applications of this scheme on the calculation of stratospheric photolysis frequencies. The strongest impact of both changes to the scheme is for small solar zenith angles. The effect of the improved treatment of the diffuse flux is most pronounced in the lower stratosphere and in the troposphere. Overall, the change in the calculated photolysis frequencies in the region of interest in the stratosphere is below about 20%, although larger deviations are found for H_2O, O_2, NO, N_2O, and HCl.

1 Introduction

Through the discovery of severe chemical ozone loss in the polar regions in winter and early spring [e.g., *WMO*, 1990, 1998] an enormous research effort was triggered which was aimed at the understanding of this phenomenon. One particular feature of the chemistry of ozone loss under these conditions is that solar zenith angles are large and the photolysis rates of photolabile compounds like, e.g., Cl_2O_2 must be accurately known [*Lary and Pyle*, 1991]. Therefore, for simulations of polar ozone loss, schemes should be employed for the calculation of photolysis frequencies which allow an accurate description of the twilight radiation field [e.g., *Lary and Pyle*, 1991; *Becker et al.*, 1998]. Furthermore, it was shown that an improved treatment of diffuse radiation field impacts on the simulation of upper stratospheric ozone [*Lary and Pyle*, 1991].

Photolysis frequencies J (in units of s^{-1}) are calculated for a particular species i from its absorption cross section σ_i, the quantum yield of the particular photolysis channel Φ and the actinic flux F (F given in units of cm^{-2} s^{-1} nm^{-1}):

$$J_i(z) = \int \sigma_i \Phi F(z) d\lambda \tag{1}$$

[*Meier et al.*, 1997], where z is altitude and λ is wavelength. Numerical schemes are employed to simulate the radiative transfer in the atmosphere and calculate $F(z)$. Here, we focus on the scheme described by *Lary and Pyle* [1991], which employs the numerical solution of the radiative transfer equation of *Meier et al.* [1982]. This scheme has been used in a variety of implementations for studies of polar lower stratospheric ozone loss [e.g., *Chipperfield et al.*, 1993; *Müller et al.*, 1994; *Lary et al.*, 1995; *Bregman et al.*, 1997; *Lutman et al.*, 1997; *Becker et al.*, 1998; *Woyke et al.*, 1999] and upper stratospheric issues [e.g., *Crutzen et al.*, 1995; *Grooß et al.*, 1999]. Here we describe an improvement of the numerics of the scheme and discuss its impact on calculated photolysis frequencies.

2 Modification to the Photolysis Scheme

2.1 The scheme of Meier et al. (1982) and Lary and Pyle (1991)

The specific photolysis scheme discussed here is based on *Meier et al.* [1982] and was originally developed by *Lary and Pyle* [1991]. Direct solar flux, multiply-scattered (diffuse) flux and the ground reflection, of both the multiply-scattered and direct solar flux, are taken into account; the direct solar flux and its ground reflection are treated using spherical geometry. Scattering is assumed to be isotropic and elastic [*Anderson and Meier*, 1979].

Central to the calculation of photolysis frequencies is the source function (or enhancement factor) S, by which the solar flux at wavelength λ at the top of the atmosphere F_0 is multiplied to obtain the total actinic flux $F(z)$ at an altitude z. Thus S is defined as

$$S = F(z)/F_0. \tag{2}$$

Including the four separate contributions to the actinic flux mentioned above, the source function S for a plane-parallel atmosphere and isotropic, elastic scattering, is defined by the radiative transfer equation [*Meier et al.*, 1982, their eq. 18]:

$$S(\tau) = \exp(-[\tau + t]/\mu_0) + 2\,A\,\mu_0 \exp(-[\tau_g + t_g]/\mu_0)\mathrm{E}_2(\Delta_g) + \int S(\tau') \left[\frac{\mathrm{E}_1(\Delta')}{2} + A\mathrm{E}_2(\Delta_g)\mathrm{E}_2(\Delta'_g)\right] d\tau'. \tag{3}$$

Here A is the ground albedo and μ_0 the cosine of the zenith angle. The scattering optical depth τ

$$\tau = \int_z^\infty \sigma^{\mathrm{scat}} n(z) dz\,, \tag{4}$$

is used as the height coordinate instead of the geometrical height z, where n is density and σ^{scat} the scattering cross section. The optical depth for pure absorption is defined analogously and is referred to as t. The optical depths at ground level are noted as τ_g and t_g. $\mathrm{E_n}$ is the $\mathrm{n^{th}}$ exponential integral [*Abramowitz and Stegun*, 1965]

$$\mathrm{E_n}(z) = \int_1^\infty \frac{e^{-zt}}{t^n} dt \tag{5}$$

and

$$\Delta' = |\tau - \tau'| + |t - t'| \quad (6)$$

$$\Delta_g = |\tau_g - \tau| + |t_g - t| \quad (7)$$

$$\Delta'_g = |\tau_g - \tau'| + |t_g - t'|. \quad (8)$$

The first term in eq. (3) describes the contribution of the direct solar radiation, the second the contribution of the ground reflection of the direct solar radiation, and the integral the contribution of the diffuse radiation and its ground reflection. To take the sphericity of the earth into account, the optical paths $[\tau + t]/\mu_0$ and $[\tau_g + t_g]/\mu_0$ are replaced by expressions calculated in spherical geometry.

Equation (3) is solved numerically using a matrix inversion technique [e.g., *Meier et al.*, 1982]. For this purpose the atmosphere is divided into N intervals; τ_n is the optical depth at the centre of the n^{th} interval and $\Delta\tau_n$ is the optical thickness of the n^{th} interval. The number of layers N is assumed to be large enough so that the source function S is constant over the integrals.

To outline the numerical solution of eq. (3) we consider for simplicity only the diffuse contribution $\tilde{S}$ without ground albedo to S:

$$\tilde{S}(\tau) = \frac{1}{2} \int S(\tau') \mathrm{E}_1(\Delta') d\tau' \quad (9)$$

where Δ' is defined in eq. (6). The numerical solution of eq. (9) for the m^{th} interval can be written as

$$\tilde{S}(\tau_m) = \frac{1}{2} \sum_{n=1}^{N} \int_{\tau_n - \Delta\tau_n/2}^{\tau_n + \Delta\tau_n/2} S(\tau'_n) \mathrm{E}_1(|\tau_m - \tau'_n| + |t_m - t'_n|) d\tau'_n \quad (10)$$

Here t is kept constant over the integration interval $\tau_n \pm \Delta\tau_n/2$. The absolute values are introduced to allow for contributions from above and below the level m. Using

$$\mathrm{E}_{\mathrm{n}-1}(x) = -\frac{d\mathrm{E}_{\mathrm{n}}(x)}{dx}. \quad (11)$$

and assuming that the thickness of the intervals is small enough for the source function S to be considered constant over each interval eq. (10) may be written as

$$\tilde{S}(\tau_m) = -\frac{1}{2} \sum_{n=1}^{N} S(\tau_n) \int_{\tau_n - \Delta\tau_n/2}^{\tau_n + \Delta\tau_n/2} \frac{d}{d\tau'_n} \Big(\mathrm{E}_2(|\tau_m - \tau'_n| + |t_m - t'_n|) \Big) d\tau'_n \quad (12)$$

Following a similar procedure including all terms in eq. (3) and using the grid points τ_n results in the matrix equation [*Meier et al.*, 1982; *Lary and Pyle*, 1991]:

$$S_m = S_{0m} + M_{mn} S_n, \tag{13}$$

where S_{0m} represents the contribution of the direct flux and its ground reflection

$$S_{0m} = \exp(-[\tau_m + t_m]/\mu_0) + 2\,A\,\mu_0 \exp(-[\tau_g + t_g]/\mu_0) \mathrm{E}_2(|\tau_g - \tau_m| + |t_g - t_m|) \tag{14}$$

and the matrix M is given as:

$$\begin{aligned} M_{mn} = \frac{1}{2} \Bigg| \mathrm{E}_2(|\tau_m - \tau_n + \frac{\Delta\tau_n}{2}| + |t_m - t_n|) - \mathrm{E}_2(|\tau_m - \tau_n - \frac{\Delta\tau_n}{2}| + |t_m - t_n|) \Bigg| \\ + A\,\mathrm{E}_2(\tau_g - \tau_m + t_g - t_m) \Bigg| \mathrm{E}_3(\tau_g - \tau_n + \frac{\Delta\tau_n}{2} + t_g - t_n) - \\ \mathrm{E}_3(\tau_g - \tau_n - \frac{\Delta\tau_n}{2} + t_g - t_n) \Bigg| . \end{aligned} \tag{15}$$

However, eq. (15) is no correct solution of eq. (10) (see section 2.2 below), so that in this formulation any contribution to the source function S from the case $n = m$ has to be neglected.

2.2 Alternative numerical solution for the source function S

There are, however, two problems with the discretisation of the integral in eq. (10) that leads to eq. (15). Firstly, $\mathrm{E}_1(x)$ diverges and $\mathrm{E}_2(|x|)$ is not differentiable at $x = 0$. Thus, for $n = m$ eq. (15) is no solution for eq. (10). Secondly, keeping t in the argument of E_2 constant ($t = t_n$) while τ varies between $\tau_n - \Delta\tau_n/2$ and $\tau_n + \Delta\tau_n/2$ can cause large errors if $n \approx m$. This is so, since $\mathrm{E}_1(x)$ diverges for $x \to 0$ and is thus very sensitive to small errors in the argument if $x \approx 0$ (that is for $n \approx m$ in eq. 15).

To obviate these two problems we adopt the following procedure. Firstly, if the case $m = n$ is treated separately – splitting the integration interval into two parts above and below zero – the problem with the pole at $x = 0$ in $\mathrm{E}_1(x)$ can be avoided. Secondly, using $\tau + t$ as the integration variable

instead of τ in eq. (3) or (9) avoids the necessity to assume $t = \text{const.}$ over the integration interval. Note that

$$\int f(\tau + t)\, d\tau = \int J(\tau) f(\tau + t)\, d(\tau + t) \tag{16}$$

where

$$J(\tau) = \frac{d\tau}{d(\tau + t)}\,. \tag{17}$$

The approximation

$$\int J(\tau) f(\tau + t)\, d(\tau + t) \approx J(\tau) \int f(\tau + t)\, d(\tau + t) \tag{18}$$

is acceptable as $J(\tau)$ varies (compared to $\mathrm{E}_1(\tau)$) only marginally with τ. Therefore we calculate the integral in eq. (10) as:

$$\tilde{S}(\tau_m) = \frac{1}{2} \sum_{n=1}^{N} \int_{\tau_n^\mathrm{e} + t_n^\mathrm{e}}^{\tau_{n+1}^\mathrm{e} + t_{n+1}^\mathrm{e}} S(\tau_n)\, J(\Delta')\, \mathrm{E}_1(\Delta')\, d\Delta', \tag{19}$$

where τ_n^e and t_n^e are the optical depths of the level edges, that is $\tau_n^\mathrm{e} = \tau_n - \Delta\tau_n/2$. Equation (19) is valid for both contributions from above ($\tau_m > \tau_n^\mathrm{e}$) and below ($\tau_m < \tau_n^\mathrm{e}$) the level m if Δ' is defined as

$$\begin{aligned} \Delta' &= \tau_m - \tau_n^\mathrm{e} + t_m - t_n^\mathrm{e} \quad \text{for} \quad \tau_m > \tau_n^\mathrm{e} \\ \Delta' &= \tau_n^\mathrm{e} - \tau_m + t_n^\mathrm{e} - t_m \quad \text{for} \quad \tau_m < \tau_n^\mathrm{e} \end{aligned}$$

These two cases can be combined using absolute values with

$$\Delta' = |\tau_m - \tau_n^\mathrm{e}| + |t_m - t_n^\mathrm{e}| \tag{20}$$

Using this formulation – and taking now all terms in eq. (3) into account – we calculate an alternative formulation for eq. (15) for M_{mn} as:

$$\begin{aligned} M_{mn} = \frac{1}{2}\, J(\tau_n) \Big| \mathrm{E}_2(|\tau_m - \tau_n^\mathrm{e}| + |t_m - t_n^\mathrm{e}|) - \mathrm{E}_2(|\tau_m - \tau_{n+1}^\mathrm{e}| + |t_m - t_{n+1}^\mathrm{e}|) \Big| \\ + A\, J(\tau_n) \mathrm{E}_2(\tau_g - \tau_m + t_g - t_m) \\ \Big| \mathrm{E}_3(\tau_g - \tau_n^\mathrm{e} + t_g - t_n^\mathrm{e}) - \mathrm{E}_3(\tau_g - \tau_{n+1}^\mathrm{e} + t_g - t_{n+1}^\mathrm{e}) \Big| \end{aligned} \tag{21}$$

if $n \neq m$. For $n = m$, splitting the integration interval into two parts above and below zero yields

$$M_{mm} = \frac{1}{2}\, J(\tau_m) \left| 2 - \mathrm{E}_2(|\tau_m - \tau_m^{\mathrm{e}}| + |t_m - t_m^{\mathrm{e}}|) - \mathrm{E}_2(|\tau_m - \tau_{m+1}^{\mathrm{e}}| + |t_m - t_{m+1}^{\mathrm{e}}|) \right| + A\, J(\tau_m) \mathrm{E}_2(\tau_g - \tau_m + t_g - t_m) \left| \mathrm{E}_3(\tau_g - \tau_m^{\mathrm{e}} + t_g - t_m^{\mathrm{e}}) - \mathrm{E}_3(\tau_g - \tau_{m+1}^{\mathrm{e}} + t_g - t_{m+1}^{\mathrm{e}}) \right| . \quad (22)$$

Here

$$J(\tau) = \left| \frac{d\tau}{d(\tau + t)} \right| = \left| 1 + \frac{\sum_i \sigma_i^{\mathrm{abs}} n_i(\tau)}{\sum_j \sigma_j^{\mathrm{scat}} n_j(\tau)} \right|^{-1} , \quad (23)$$

where σ_i^{abs} is the absorption cross section of species i, σ_i^{scat} its scattering cross section, and n_i its density.

3 Results of the Numerical Experiments

To investigate the impact of the improved numerical solution of the integral in eq. (3) through the formulation in eqs. (21) and (22) we compare the stratospheric photolysis frequencies calculated using this scheme against those resulting from the original formulation eq. (15). We employ a temperature and ozone mixing-ratio profile according to the U.S. Standard atmosphere and the currently recommended set of absorption cross sections [*DeMore et al.*, 1997]. Solar input in the wave-length range of 420-850 nm and 175-420 nm is from *WMO* [1986] and *Lean et al.* [1997] respectively. For the present calculations, the model top is located at 80 km (0.01 hPa), the model bottom is at the sea level, we have assumed an average ground albedo of 0.4; the model top is located at 80 km (0.01 hPa) and the standard number of vertical levels is $N = 30$.

For completeness, we also investigate the impact of a programming error in the calculation of the optical depth which was present in the version of the code in question here prior to 1998 [e.g., *Müller et al.*, 1994; *Crutzen et al.*, 1995], but which has been corrected since [*Becker et al.*, 1998; *Woyke et al.*, 1999; *Grooß et al.*, 1999]: The optical depth t (compare eq. 4) between the model level i and the top of the atmosphere due to oxygen and ozone

absorption is calculated from

$$t(i,\chi,\lambda) = \sum_{j=i}^{N} \Delta z(i,j,\chi) \cdot \left\{ [\mathrm{O_3}(j)]\ \sigma_{\mathrm{O_3}}(\lambda, T_j) + [\mathrm{O_2}(j)]\ \sigma_{\mathrm{O_2}}(\lambda, T_j) \right\} \quad (24)$$

where $[\mathrm{O_2}(j)]$ and $[\mathrm{O_3}(j)]$ are the oxygen and ozone molecule concentrations in the j^{th} model level, $\sigma_{\mathrm{O_2}}$ and $\sigma_{\mathrm{O_3}}$ are the absorption cross sections of oxygen and ozone at wavelength λ, T_j is the temperature of the j^{th} model level, $\Delta z(i,j,\chi)$ is the light path length through the j^{th} model level at zenith angle χ, and N denotes the index of the top model level. In the old code version, the optical depth calculation for zenith angles $\chi < 90^\circ$ used T_i instead of T_j, i.e. the temperature dependence of the absorption cross sections was treated incorrectly.

To investigate the impact of the changes to the photolysis scheme we have conducted the following model calculations. Calculation A: without the improved integral solution as described in the previous section, calculation B: with the incorrect temperature dependence of $\sigma_{\mathrm{O_2}}$ and $\sigma_{\mathrm{O_3}}$ (compare eq. 24), calculation A+B: a combination of A and B, that is the model version as it was used in earlier studies prior to 1998 [e.g., *Müller et al.*, 1994; *Crutzen et al.*, 1995]. The new version with all corrections and improvements is used as the reference case.

The results of the intercomparison between the different cases are shown in Figure 1 for the photolysis of four species which photolyse in different wavelength regimes (namely, $\mathrm{O_2}$, $\mathrm{O_3}[\rightarrow \mathrm{O}(^1\mathrm{D})]$, $\mathrm{Cl_2O_2}$, and $\mathrm{HNO_3}$). In addition, the results for several other photolysis rates of stratospheric relevance at a pressure level in the upper (1 hPa) and in the lower (80 hPa) stratosphere are summarised in Table 1. The effect of the calculation without the improved integral solution (calculation A, dotted lines) is largest in the lower stratosphere. For 30 model levels, the results of calculation A yield about 10-20% lower photolysis rates in the lower stratosphere depending on the chemical species (Table 1). With increasing number of model levels, this deviation decreases, namely by about a factor of two for 100 model levels and a factor of four for 250 model levels. This behaviour reflects the slow convergence with increasing number of model levels in the old model version (Figure 2). The impact of the incorrect temperature dependence of $\sigma_{\mathrm{O_2}}$ and $\sigma_{\mathrm{O_3}}$ is also shown in Figure 1 (calculation B, dashed lines) as well as in Table 1. Significant deviations are found for the photolysis rates of $\mathrm{O_2}$, $\mathrm{H_2O}$, HCl, NO, and $\mathrm{N_2O}$ that absorb solar radiation in the UV-C range ($\lambda < 280$ nm).

Unlike in calculation A, an increase of the model resolution has a negligible effect here.

The impact of the changes to the photolysis scheme further depends on the solar zenith angle (Figures 3 and 4). Both the effect of the improved integral solution (calculation A) (Figure 3) and of the incorrect temperature dependence of σ_{O_2} and σ_{O_3} (calculation B) (Figure 4) are most pronounced for small zenith angles.

To assess these results, not only the relative difference between calculations A, B, and the reference calculation but also the relevance for atmospheric chemistry has to be considered: e.g., the effect of calculation B is not very important in the lower stratosphere, since the radiation in the UV-C wavelength range is already absorbed in the air masses above. A relative increase of a factor of three in $J(H_2O)$ or a 10% increase in $J(O_2)$ is not relevant because these rates are below any level of significance in the lower stratosphere.

Calculations (not shown) investigating the impact of the improved photolysis scheme in the polar lower stratosphere showed that simulated ozone loss rates [*Becker et al.*, 1998] are not significantly altered if the improved scheme is introduced. However, the impact of the improvements (calculation B) for studies of the upper stratosphere is not negligible. This is shown in calculations of the upper stratospheric ozone budget [*Grooß et al.*, 1999]. A 10% bias in $J(O_2)$ in previous calculations [*Crutzen et al.*, 1995] caused an overestimate of the ozone production rates. This effect was partially compensated in the study of *Crutzen et al.* [1995] by the bias in $J(H_2O)$, since in the upper stratosphere and mesosphere H_2O photolysis is a major source of HO_x radicals which dominate the ozone destruction cycles at these altitudes.

We have moreover compared (Figure 5) the photolysis frequency of NO_2 calculated from the old and the improved model version with the photolysis benchmark developed by *Stolarski* [1995]. Calculations were performed for a solar zenith angle of zero degree and for a ground albedo of 0.3; it is unclear, however, in how far other model assumptions (e.g., solar flux) resemble those of the photolysis benchmark of *Stolarski* [1995]. Also shown in Figure 5 (grey shaded area) are the values calculated by all thirteen models participating in the 1995 model intercomparison [*Stolarski*, 1995]. Throughout the considered altitude range (0-60 km), the results for the reference case are within 5 % of the 1995 photolysis benchmark. The improvement through the the new integral solution described in section 2.2, becomes increasingly obvious towards lower altitudes (in particular in the troposphere), that is in a regime

where the importance of multiple scattering is increasing.

4 Conclusions

We have presented an improvement of the treatment of the diffuse actinic flux in the widely used stratospheric photolysis scheme by *Meier et al.* [1982] and *Lary and Pyle* [1991]. We have discussed the impact of this improvement on the calculation of stratospheric photolysis frequencies. Moreover, the influence of a coding error, present in earlier studies using this scheme [e.g., *Müller et al.*, 1994; *Crutzen et al.*, 1995] has been addressed. The strongest impact of both changes to the scheme is for small solar zenith angles. The effect of the improved treatment of the diffuse flux is most pronounced in the lower stratosphere and in the troposphere. Overall, the change in the calculated photolysis frequencies in the region of interest in the stratosphere is below about 20%, although there are some exceptions. Most strongly affected are the photolysis frequencies of H_2O, O_2, NO, N_2O, and HCl.

Acknowledgements

We thank David Lary for supplying his original code several years ago and for his continuous help and support with updates. We are grateful to Jürgen Ankenbrand for programming support. Thanks to two anonymous referees for their constructive, helpful suggestions. This work was partly supported by the German Bundesministerium für Bildung, Wissenschaft, Forschung und Technologie.

Table 1: Calculation for all model photolysis frequencies and their relative deviation for two pressure levels (80 and 1 hPa) and for calculation A (without the improved integral solution as described in section 2.2) and for calculation B (with the incorrect temperature dependence of σ_{O_2} and σ_{O_3} (compare eq. 24). The calculations are based on 30 model levels, top pressure level 0.01 hPa (80 km), albedo=0.4, and 60° solar zenith angle.

Photolysis Reaction	Pressure = 80hPa rate [s^{-1}]	Deviation [%] A	B	Pressure = 1hPa rate [s^{-1}]	Deviation [%] A	B
$O_2 \rightarrow O+O$	4.46E-15	-14.9	10.2	6.08E-10	-0.5	10.3
$O_3 \rightarrow O+O_2$	5.38E-04	-2.9	0.0	1.01E-03	-0.7	0.0
$O_3 \rightarrow O(^1D)+O_2$	1.75E-05	-10.9	1.5	3.91E-03	-0.1	0.0
$H_2O_2 \rightarrow 2\ OH$	7.65E-06	-15.8	0.3	3.30E-05	-2.1	0.0
$H_2O \rightarrow H+OH$	2.82E-15	-16.6	337.8	1.96E-09	-0.5	145.5
$NO \rightarrow N+O$	0.0	–	–	3.15E-07	-0.5	95.0
$NO_2 \rightarrow NO+O$	1.32E-02	-11.7	0.0	1.32E-02	-6.7	0.0
$NO_3 \rightarrow NO+O_2$	2.14E-01	-2.0	0.0	2.16E-01	-0.8	0.0
$NO_3 \rightarrow NO_2+O$	2.95E-02	-1.1	0.0	2.74E-02	-0.3	0.0
$N_2O_5 \rightarrow NO_2+NO_3$	2.45E-05	-15.5	0.3	5.03E-04	-1.1	0.0
$HNO_3 \rightarrow OH+NO_2$	4.56E-07	-14.1	0.8	8.26E-05	-0.6	5.0
$HO_2NO_2 \rightarrow HO_2+NO_2$	8.78E-06	-15.4	0.5	3.04E-04	-0.5	1.4
$N_2O \rightarrow N+NO$	7.62E-12	-15.5	25.4	4.48E-07	-0.6	11.2
$Cl_2 \rightarrow 2\ Cl$	3.54E-03	-14.0	0.1	3.81E-03	-7.2	0.0
$Cl_2O_2 \rightarrow Cl+ClO_2$	2.01E-03	-14.6	0.2	5.09E-03	-3.1	0.0
$OClO \rightarrow ClO+O$	1.25E-01	-11.8	0.0	1.27E-01	-6.6	0.0
$HOCl \rightarrow Cl+OH$	3.50E-04	-15.4	0.1	5.18E-04	-5.5	0.0
$ClNO_2 \rightarrow Cl+NO_2$	5.29E-04	-15.7	0.2	1.37E-03	-3.3	0.5
$ClONO_2 \rightarrow Cl+NO_3$	5.44E-05	-13.5	0.1	5.42E-04	-1.1	0.1
$HCl \rightarrow H+Cl$	8.50E-12	-15.3	26.8	4.56E-07	-0.6	17.9
$Br_2 \rightarrow 2\ Br$	4.62E-02	-5.2	0.0	4.57E-02	-2.8	0.0
$BrO \rightarrow Br + O$	5.74E-02	-15.8	0.1	6.11E-02	-8.1	0.0
$HOBr \rightarrow Br+OH$	2.91E-03	-12.1	0.0	3.41E-03	-5.9	0.0
$BrONO_2 \rightarrow BrO+NO_2$	1.89E-03	-11.6	0.1	2.69E-03	-4.6	0.0
$BrCl \rightarrow Br+Cl$	1.55E-02	-8.4	0.0	1.54E-02	-4.9	0.0
$CH_2O \rightarrow H+HCO$	7.15E-05	-16.4	0.1	8.10E-05	-7.7	0.0
$CH_2O \rightarrow H_2+CO$	4.11E-05	-16.0	0.4	6.78E-05	-4.3	0.0
$CH_3OOH \rightarrow CH_3O+OH$	7.66E-06	-15.6	0.2	4.09E-05	-1.7	0.0
$CH_3OCl \rightarrow CH_3O+Cl$	1.30E-04	-13.6	0.1	1.86E-04	-5.2	0.0

Figures

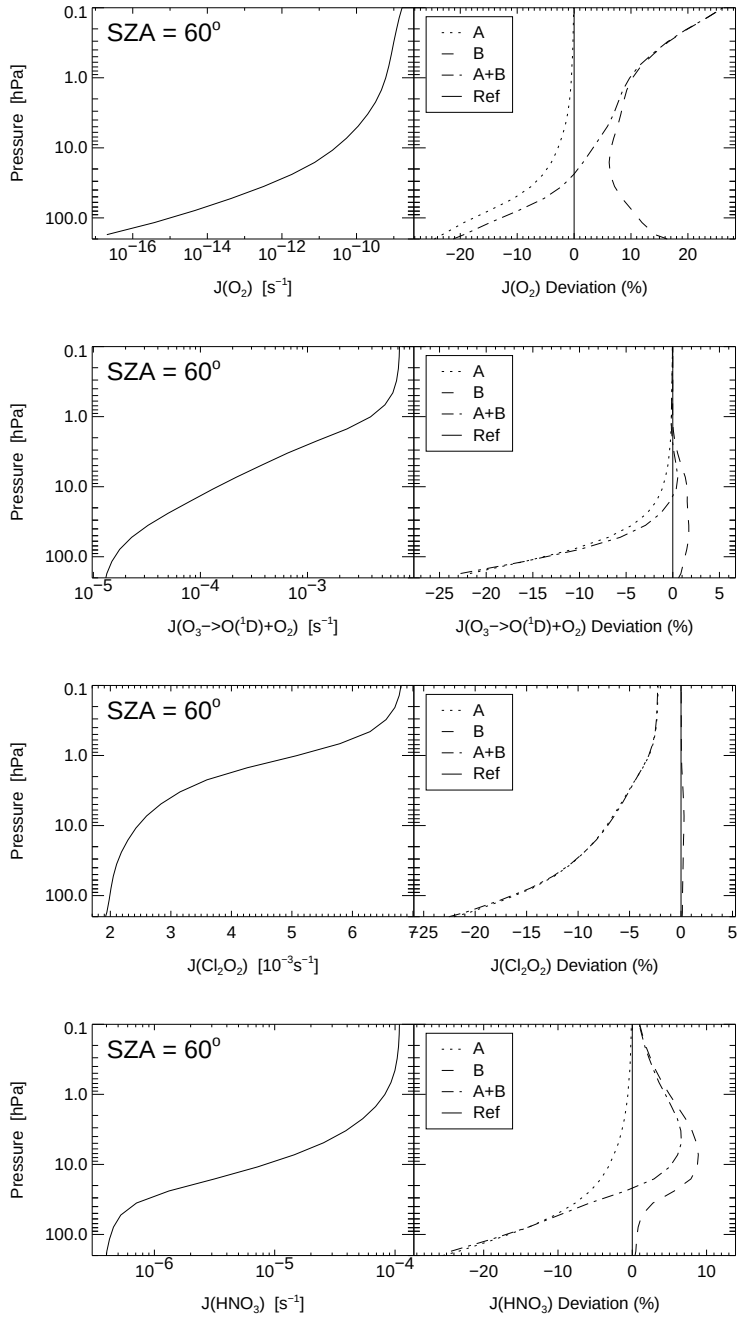

Figure 1: Calculation of the photolysis frequencies for O_2, $O_3[\rightarrow O(^1D)]$, Cl_2O_2, and HNO_3 as a function of pressure (altitude). The left panels show the absolute photolysis frequency for the reference calculation, the right panel depicts the relative difference for model calculations A (without the improved integral solution as described in section 2.2), B (with the incorrect temperature dependence of σ_{O_2} and σ_{O_3} (compare eq. 24), and A+B (see text for further details). The calculation was performed with 30 model levels, top pressure level 0.01 hPa (80 km), albedo=0.4, and 60° solar zenith angle.

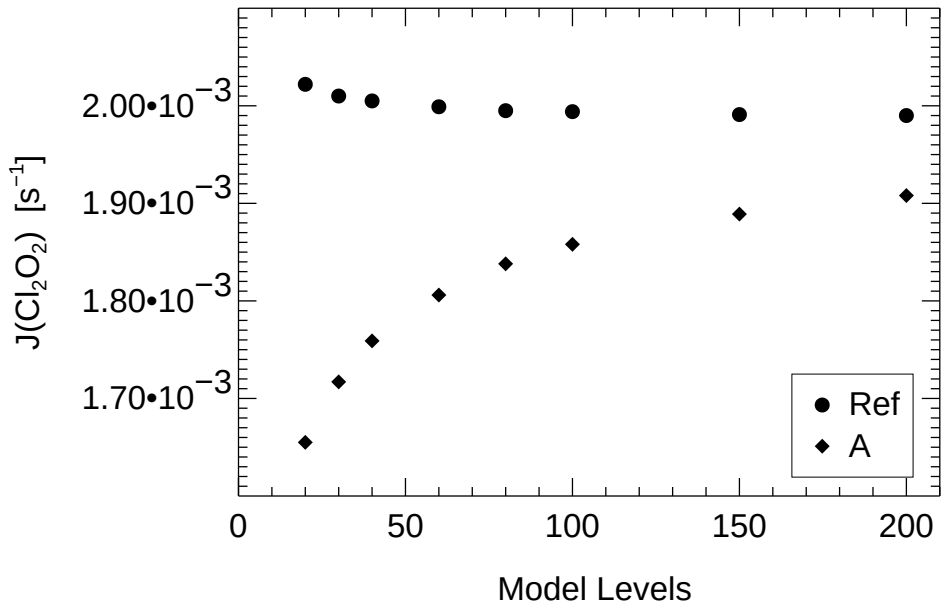

Figure 2: The Cl_2O_2 photolysis frequency $J(Cl_2O_2)$ at 80 hPa for a zenith angle of 80° versus the number of levels used for numerical evaluation of the integrals; comparison of results obtained with eq. (15) (case A, diamonds) and results obtained with eq. (21) and (22) (reference case, circles).

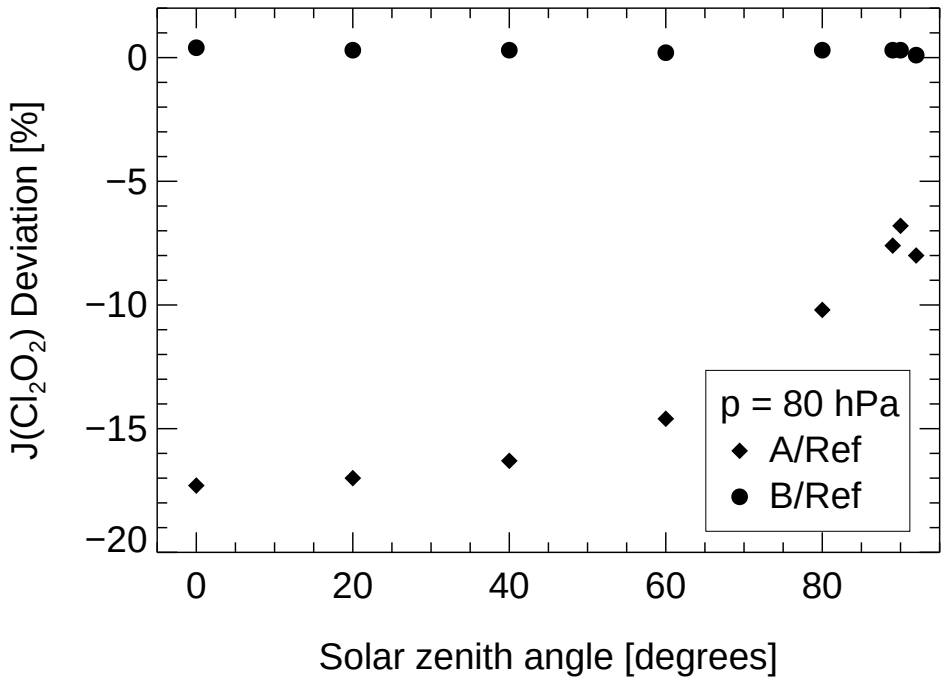

Figure 3: The impact of the improvements of the scheme in the lower stratosphere. Shown is the deviation of $J(Cl_2O_2)$ for calculations A (diamonds) and B (solid circles) (see Fig. 1 and text) from the reference case (i.e., the improved scheme) in dependence of the solar zenith angle. Values are given for 80 hPa.

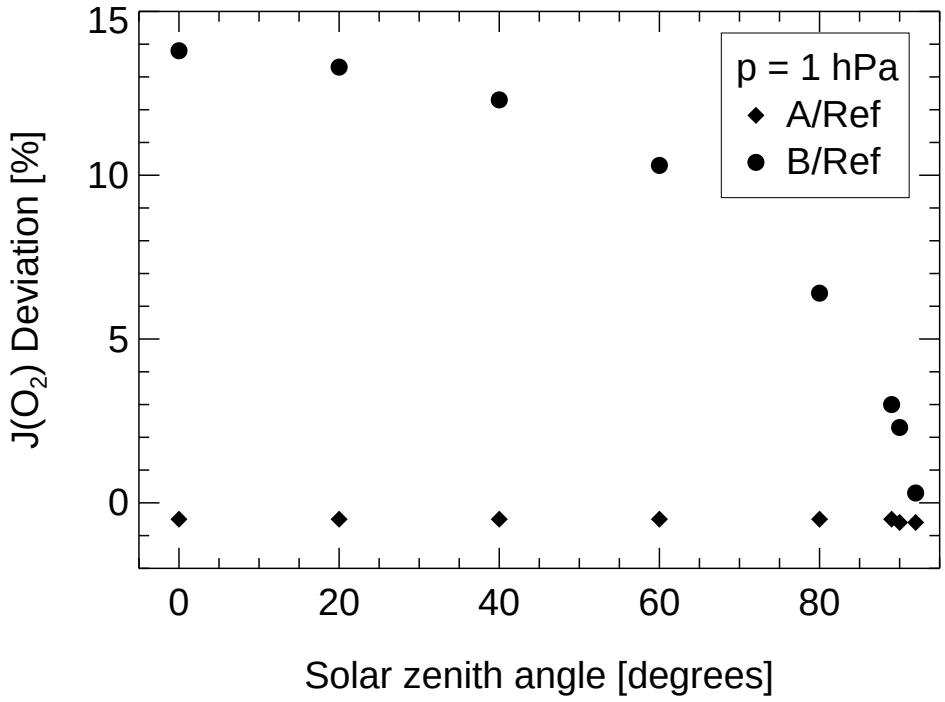

Figure 4: The impact of the improvements of the scheme in the upper stratosphere. Shown is the deviation of $J(O_2)$ for calculations A (diamonds) and B (solid circles) (see Fig. 1 and text) from the reference case (i.e., the improved scheme) in dependence of the solar zenith angle. Values are given for 1 hPa.

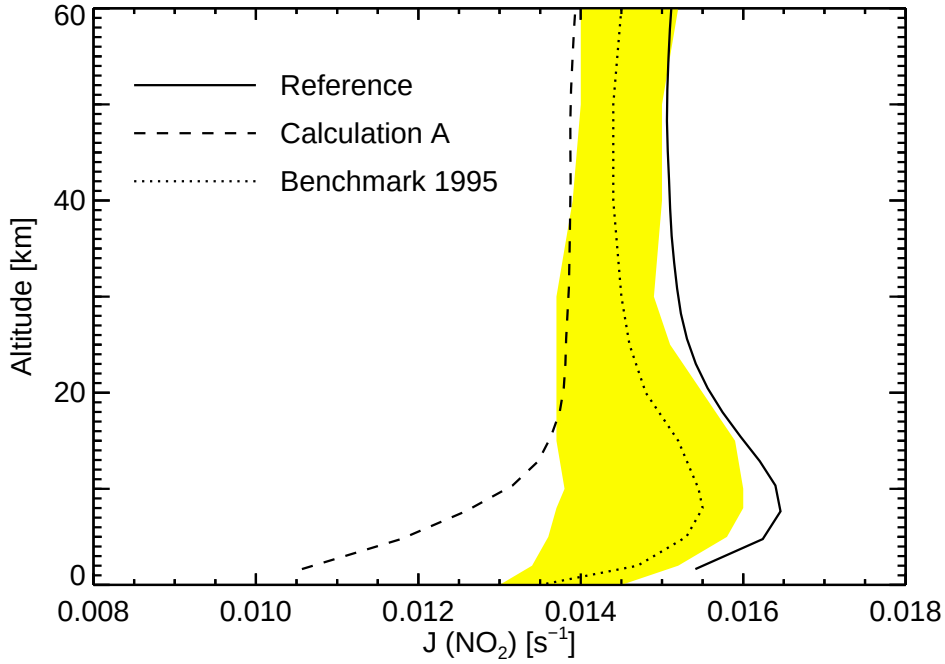

Figure 5: Comparison of the photolysis frequency of NO_2 for the reference calculation (solid line) and calculation A (without the improved integral solution described in section 2.2, dashed line) with the photolysis benchmark developed by *Stolarski* [1995] (dotted line). The grey shaded region indicates the spread of the various model results in the photolysis scheme intercomparison of *Stolarski* [1995]. Calculations are for clear sky, albedo 0.3 and solar zenith angle 0°.

References

Abramowitz, M., and I. A. Stegun, eds., *Handbook of Mathematical Functions*, Dover Publications, New York, 1965.

Anderson, D. E., and R. R. Meier, The effects of anisotropic multiple scattering on solar radiation in the troposphere and stratosphere, *Appl. Optics*, *18*, 1955, 1979.

Becker, G., R. Müller, D. S. McKenna, M. Rex, and K. S. Carslaw, Ozone loss rates in the Arctic stratosphere in the winter 1991/92: Model calculations compared with Match results, *Geophys. Res. Lett.*, *25*, 4325–4328, 1998.

Bregman, A., M. van den Broek, K. S. Carslaw, R. Müller, T. Peter, M. P. Scheele, and J. Lelieveld, Ozone depletion in the late winter lower arctic stratosphere: Observations and model results, *J. Geophys. Res.*, *102*, 10815–10828, 1997.

Chipperfield, M. P., D. Cariolle, P. Simon, R. Ramaroson, and D. J. Lary, A three-dimensional modeling study of trace species in the Arctic lower stratosphere during winter 1989-1990, *J. Geophys. Res.*, *98*, 7199–7218, 1993.

Crutzen, P. J., J.-U. Grooß, C. Brühl, R. Müller, and J. M. Russell III, A reevaluation of the ozone budget with HALOE UARS data: No evidence for the ozone deficit, *Science*, *268*, 705–708, 1995.

DeMore, W. B., S. P. Sander, D. M. Golden, R. F. Hampson, M. J. Kurylo, C. J. Howard, A. R. Ravishankara, C. E. Kolb, and M. J. Molina, Chemical kinetics and photochemical data for use in stratospheric modeling, JPL publication 97-4, 1997.

Grooß, J.-U., R. Müller, G. Becker, D. S. McKenna, and P. J. Crutzen, An update of the upper stratospheric ozone budget calculations based on HALOE data, *J. Atmos. Chem.*, *34*, 171–183, 1999.

Lary, D. J., and J. A. Pyle, Diffuse radiation, twilight, and photochemistry - I, *J. Atmos. Chem.*, *13*, 373–406, 1991.

Lary, D. J., M. P. Chipperfield, and R. Toumi, The potential impact of the reaction OH+ClO $\rightarrow$ HCl+O_2 on polar ozone photochemistry, *J. Atmos. Chem.*, *21*, 61–79, 1995.

Lean, J. L., G. J. Rottman, H. L. Kyle, T. N. Woods, J. R. Hickey, and L. C. Puga, Detection and parameterization of variations in solar mid- and near-ultraviolet radiation (200-400 nm), *J. Geophys. Res.*, *102*, 29939–29956, 1997.

Lutman, E. R., J. A. Pyle, M. P. Chipperfield, D. J. Lary, I. Kilbane-Dawe, J. W. Waters, and N. Larsen, Three-dimensional studies of the 1991/1992 northern hemisphere winter using domain-filling trajectories with chemistry, *J. Geophys. Res.*, *102*, 1479–1488, 1997.

Meier, R. R., D. E. Anderson Jr., and M. Nicolet, Radiation Field in the Troposphere and Stratosphere from 240-1000 nm -I: General Analysis, *Planet. Space Sci.*, *30*, 923–933, 1982.

Meier, R. R., G. Anderson, C. Cantrell, L. Hall, J. Lean, K. Minschwaner, R. Shetter, E. Shettle, and K. Stamnes, Actinic Radiation in the terrestrial atmosphere, *J. Atmos. Solar-Terr. Phys.*, *59*, 2111–2157, 1997.

Müller, R., P. J. Crutzen, H. Oelhaf, G. P. Adrian, T. v. Clarmann, A. Wegner, U. Schmidt, and D. Lary, Chlorine chemistry and the potential for ozone depletion in the Arctic stratosphere in the winter of 1991/92, *Geophys. Res. Lett.*, *21*, 1427–1430, 1994.

Stolarski, R. S., 1995 Scientific assessment of the atmospheric effects of stratospheric aircraft, *NASA Reference Publication 1381*, NASA, 1995.

WMO, *Scientific assessment of ozone depletion: 1985*, Report No. 16, Geneva, 1986.

WMO, *Scientific assessment of ozone depletion: 1989*, Report No. 20, Geneva, 1990.

WMO, *Scientific assessment of ozone depletion: 1998*, Report No. 44, Geneva, 1998.

Woyke, T., R. Müller, F. Stroh, D. S. McKenna, A. Engel, J. J. Margitan, M. Rex, and K. S. Carslaw, A test of our understanding of the ozone chemistry in the Arctic polar vortex based on in-situ measurements of ClO, BrO, and O_3 in the 1994/95 winter, *J. Geophys. Res.*, *104*, 18755–18768, 1999.